RESEARCH ARTICLE

ADVANCED OPTICAL MATERIALS
www.advopticalmat.de

Quantifying Spin-Charge Conversion Mechanisms for THz Emission in Magnetic Multilayers

Yunxiu Zhao, Anabil Gayen, Lin Huang, Xiao You, Nguyen Le Thi, Qoimatul Mustaghfiroh, Fathiya Rahmani, Prashant Vijay Gaikwad, Pham Duc Huyen Yen, Je-Ho Shim, Dong Eon Kim, Hee Jun Shin, Jaehun Park, Caihua Wan, Ou Xiang, Hong-Guang Piao, Kyung-Ho Kim, Junhyeok Bang, Hyun Seok Lee, Kyung Wan Kim,* and Dong-Hyun Kim**

Ultrafast control of both electric and spin currents triggered by femtosecond laser pulse has attracted much attention due to future applications for broadband THz emitter as well as high-speed spintronic devices. Optically generated spin current is converted to charge current via multiple spin-charge conversion mechanisms, generating THz wave emission in magnetic multilayers. However, to date, quantitative and comparative investigation of THz emission originating from spin-charge conversion mechanisms has not yet been fully explored. Here, direct and straightforward nondestructive probing to measure THz emission is provided at original Co/Pt and Co/Ta interfaces embedded in Pt/Co/Ta multilayers with polarization analysis of both optical pump and THz emission. These results allow a fundamental understanding of various spin-charge conversion phenomena, which is a key basis for future spintronic THz source development.

1. Introduction

Terahertz (THz) spintronics based on magnetic materials has attracted much attention for potential applications.[1–5] When magnetic materials are irradiated by femtosecond laser pulse, THz pulse should be emitted by time-dependent magnetization change, mostly observed as photoinduced ultrafast demagnetization.[6–8] The THz emission by ultrafast demagnetization is universally observed in magnetic films,[9,10] which is well explained based on the Maxwell equation. The THz emission by the ultrafast demagnetization becomes dominant for relatively thick ferromagnetic layer (> 20 nm), while it becomes negligible for thin ferromagnetic films with more intriguing interface effect.[9]

In case of thin magnetic multilayer films, it has been reported that there exists a spin-charge conversion phenomenon, where ultrafast spin dynamics results in charge dynamics on a sub-ps timescale, generating THz emission[11,12] and efficiently working as a broadband THz emitter.[3,15] Several spin-charge conversion mechanisms originated from an interface in multilayer structure for spintronic THz emitters are proposed such as inverse spin Hall

Y. Zhao, A. Gayen, L. Huang, N. L. Thi, Q. Mustaghfiroh, F. Rahmani, P. V. Gaikwad, P. D. H. Yen, K.-H. Kim, J. Bang, H. S. Lee, K. W. Kim, D.-H. Kim
Department of Physics
Chungbuk National University
Cheongju 28644, South Korea
E-mail: kyungwan@chungbuk.ac.kr; donghyun@chungbuk.ac.kr

Y. Zhao, X. You
School of Engineering
Westlake University
Hangzhou 310024, China

L. Huang
Key Laboratory of Advanced Materials
School of Materials Science and Engineering
Tsinghua University
Beijing 100084, China

The ORCID identification number(s) for the author(s) of this article can be found under https://doi.org/10.1002/adom.202302571

DOI: 10.1002/adom.202302571

J.-H. Shim, D. E. Kim
Department of Physics and Center for Attosecond Science and Technology
POSTECH
Pohang 37673, South Korea

J.-H. Shim, H.-G. Piao
Department of Physics
Yanbian University
Yanbian 133002, China
E-mail: hgpiao@ybu.edu.cn

H. J. Shin, J. Park
Pohang Accelerator Laboratory
POSTECH
Pohang 37673, South Korea

C. Wan
Institute of Physics
Chinese Academy of Science
Beijing 100190, China

O. Xiang
Manufacturing department
Yangtze Memory Technologies Co., Ltd. (YMTC)
Wuhan 430073, China

effect (ISHE),[13–16] inverse Rashba–Edelstein effect (IREE),[17,18] and inverse spin-orbit torque (ISOT).[19–21] To explore the THz emission by ISHE, IREE, and ISOT, numerous studies have been carried out mostly for magnetic multilayers with an interface between magnetic and various nonmagnetic materials. For instance, THz emission by ISHE has been reported for ferromagnetic/heavy-metal heterostructures,[22] ferromagnet/semiconductor heterostructures,[23] and transition-metal/Pt multilayers.[24] THz emission by IREE has been reported for Fe/Ag/Bi film[17] and CoFeB/Ag/Bi film.[18] THz emission by ISOT has also been reported for Co/Pt-based multilayer with space inversion symmetry broken.[19–21]

Since these mechanisms coexist in THz emission behavior for magnetic multilayers, to distinguish those mechanisms based on quantitative and comparative analysis in multilayer systems still remain a scientific challenge. In particular, ISHE and IREE produces the THz emission with the same polarization, letting the separation of contributions from these two mechanisms become challenging. Moreover, it should be mentioned that THz emission by ISOT depends on a pump laser helicity, while THz emission by IREE and ISHE do not. Therefore, systematic approach with controlling laser polarization together with quantitative analysis of THz field polarization is required to quantitatively and comparatively investigate the coexisting THz emission mechanisms.

In this work, we have carried out an optical pump and THz emission probe experiment on an ultrafast timescale to investigate pump-polarization-dependent THz emission for Pt/Co and Pt/Co/Ta multilayer films. Spin-charge conversion mechanisms for THz emission are distinguished based on the estimation of original THz emission at each interface composing multilayers, where the contributions from ISHE, IREE, and ISOT mechanisms are quantified at Co/Pt and Co/Ta interfaces. Our finding provides a comparative and quantitative way to separately understand different mechanisms inevitably coexisting in THz emission from various magnetic multilayers, which is a key aspect in the realization of broadband spintronic THz emitter.

2. Results and Discussion

Pt(5 nm)/Co(3 nm)/MgO(2 nm) and Pt(5 nm)/Co(3 nm)/Ta (5 nm)/MgO(2 nm) multilayer films are grown on 0.5-mm thick sapphire substrate by magnetron sputtering with sputtering pressure of 7 mTorr. The MgO layer is selected as a protection layer, insulating any charge current into the layer. Sapphire and MgO are optically transparent, allowing laser pulse to mostly transmit. Co layer thickness is fixed to be 3 nm, where it is expected that THz emission is mostly dominated by the spin-charge conversion at the interface rather than from the ultrafast demagnetization.[9] Ta layer is inserted into one of the samples to investigate the Co/Ta interface contribution with comparison to the Co/Pt interface, known to have an opposite sign of the spin Hall angle.[25] The structural information about the films by high-resolution cross-sectional transmission electron microscopy is described in Section S3 (Supporting Information). Hysteresis loops of samples measured on the film plane are plotted in **Figure 1a**, which confirms the in-plane magnetic anisotropy on the film plane for both the samples.

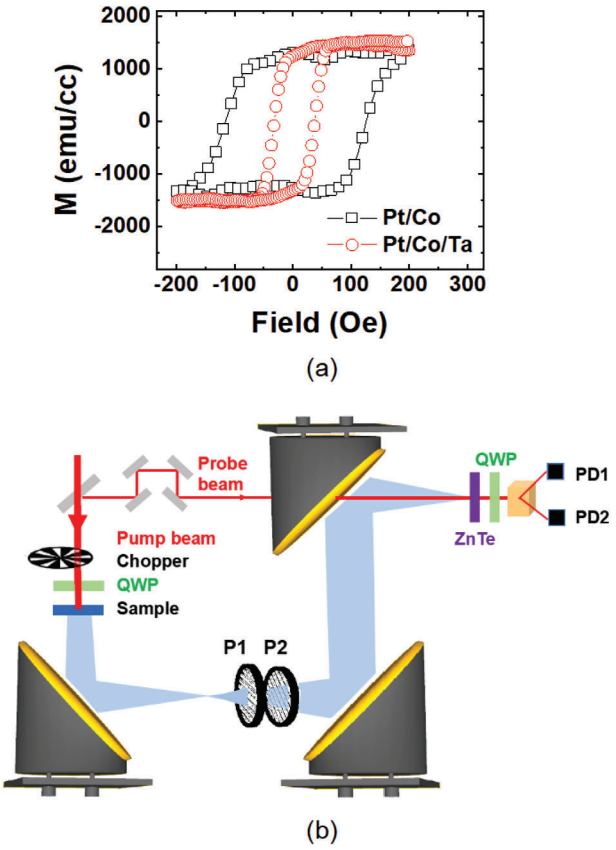

Figure 1. a) M-H hysteresis loops of Co/Pt (open square) and Pt/Co/Ta (open circle) multilayers. b) Schematic diagram of THz emission setup. The pump beam passes through the chopper and QWP (quarter-wave plate), exciting the sample. THz pulse is generated and passes through P1, P2 (wire grid polarizer), collimated by a parabolic mirror, and refocused on ZnTe crystal. The probe beam undergoes a time delay, and travels through ZnTe crystal, QWP, and two photodiodes (PD1 and PD2).

The THz emission experiment was carried out at Pohang Accelerator Laboratory (PAL) in Korea. Ti: Sapphire regenerative amplifier with the wavelength of 800 nm, 20 nm bandwidth, 120 fs pulse duration, and 1 kHz repetition rate was used as the femtosecond laser source. The pump laser spot size is ≈5 mm with incidence normal to the film surface. The pump polarization is selected to be linear, left-circularly polarized (LCP), or right-circularly polarized (RCP). The pump fluence was varied between 0.5 and 1.68 mJ cm^{-2}, where the results exhibit a similar trend in this fluence range, with THz emission roughly proportional to the fluence. The data with the maximal fluence of 1.68 mJ cm^{-2} will be representatively shown. The emitted THz pulse is focused onto a 1 mm-thick ZnTe (110) crystal by parabolic mirrors and detected via an electro-optic sampling technique. The details of the THz emission detection experiment are described elsewhere.[10,26] To explore the polarization-resolved THz emission with a fixed ZnTe crystal axis, two wire grid polarizers (WGP) with a relative angle of 45° have been adopted to selectively pass the THz emission either with an electric field along the x-axis (E_x) or the y-axis (E_y).[27] The schematic diagram of the setup is shown in Figure 1b. In-plane external magnetic field up to 450 Oe is applied. All experiments are carried out inside the

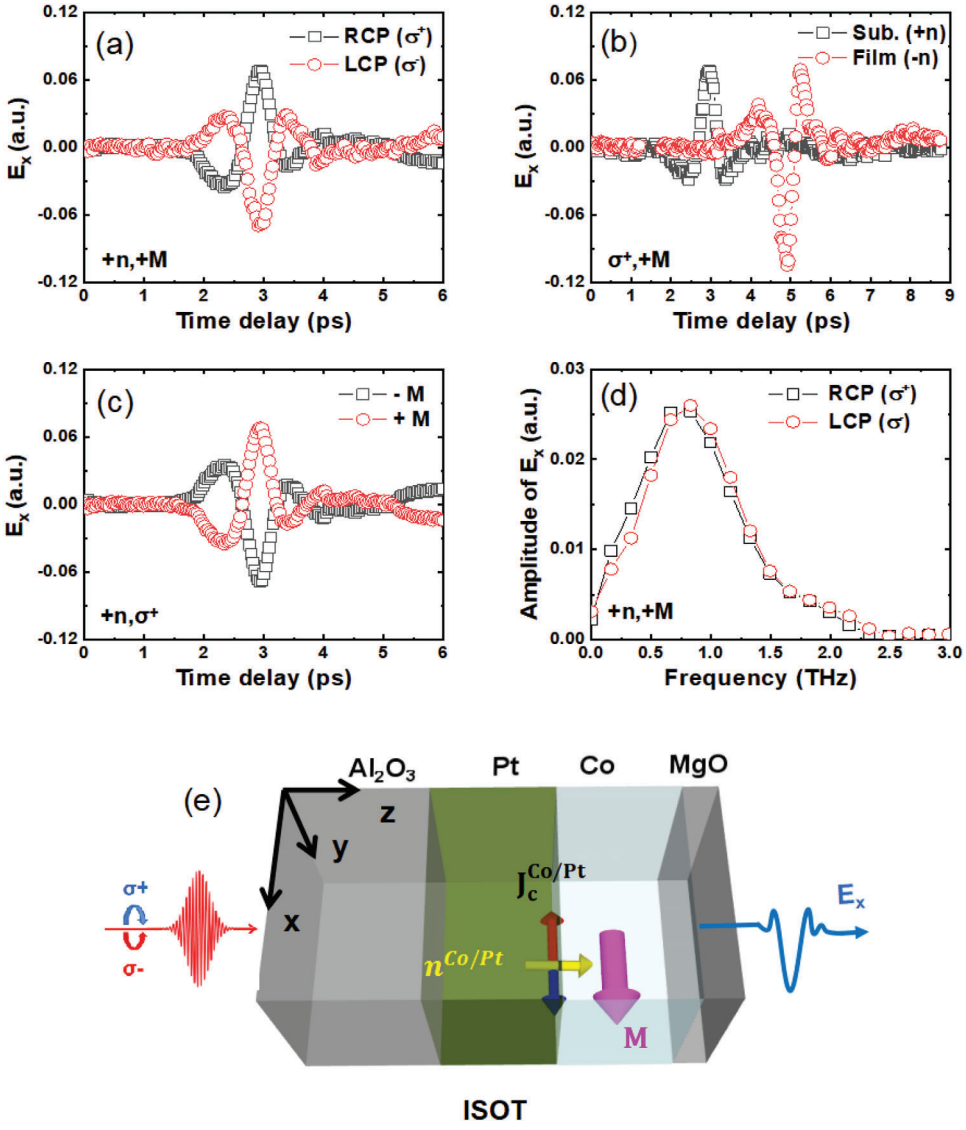

Figure 2. a) E_x generated by LCP (σ^-) and RCP (σ^+) for the case of $+\mathbf{n}$ and $+\mathbf{M}$. b) E_x with pump incident from the substrate ($+n$) and the film side ($-n$) for the case of σ^+ and $+\mathbf{M}$. c) E_x with $+\mathbf{M}$ and $-\mathbf{M}$ for the case of $+n$ and σ^+. d) FFT of E_x for LCP and RCP pump. e) Schematic diagram of ISOT with pump, sample, and THz emission geometry. LCP (σ^-, red)/RCP (σ^+, blue) pump excites the sample, leading to induced charge current, $J_c^{Co/Pt}$ by LCP (red) and RCP (blue). Polar unit vector $n^{Co/Pt}$ normal to the interface, M. THz emission along the x-axis is denoted as E_x.

dry air chamber at room temperature with a relative humidity of 1.0% to avoid the THz absorption by water vapor.

First, pump-polarization-dependent THz emission behavior is observed with LCP/RCP pump polarization for the Pt/Co bilayer film, from which pure ISOT contribution is estimated by analyzing E_x. **Figure 2** depicts THz electric field profile along the x-axis with a variation of pump helicity (LCP/RCP) (Figure 2a), pumping direction (film-/substrate-side) (Figure 2b), external magnetic field (Figure 2c). In Figure 2d, the FFT of THz emission profiles in the case of RCP and LCP pumps, are plotted, where the almost same FFT spectra are observed. Symmetric THz emission profiles by LCP/RCP pump indicate the THz emission in both cases originated by the same mechanism (ISOT). As in Figure 2a, the electric field profile of THz emission along the x-axis (E_x) by LCP/RCP pump exhibits a symmetrically opposite phase when magnetically saturated along the +x direction ($+\mathbf{M}$) by +450 Oe external field. Considering that ISOT is described by the formula: $\mathbf{J}_c = \chi \mathbf{n} \times [\mathbf{M} \times \boldsymbol{\sigma}] I$[19], where J_c is an induced charge current, χ is a spin-orbit coupling strength, $\boldsymbol{n}$ is the polar unit vector normal to the interface, $\boldsymbol{\sigma}$ represents pump helicity, $\boldsymbol{M}$ is a sample magnetization, and I is the pump intensity. It is expected to have an opposite J_c by switching between LCP (σ^-) and RCP (σ^+), as demonstrated in the figure. The geometry of the sample and J_c, $\boldsymbol{n}$, $\boldsymbol{\sigma}$, and $\boldsymbol{M}$ are illustrated in Figure 2e.

In Figure 2b, electric field profile of THz emission by flipping the sample is plotted, where $\boldsymbol{n}$ is oppositely switched, and accordingly, E_x changes the sign. THz field profile phase is delayed when the sample is hit on the film-side ($-\boldsymbol{n}$) due to the increased optical path mainly by the 0.5-mm thick sapphire substrate for THz pulse generated at the Co/Pt interface. THz emission

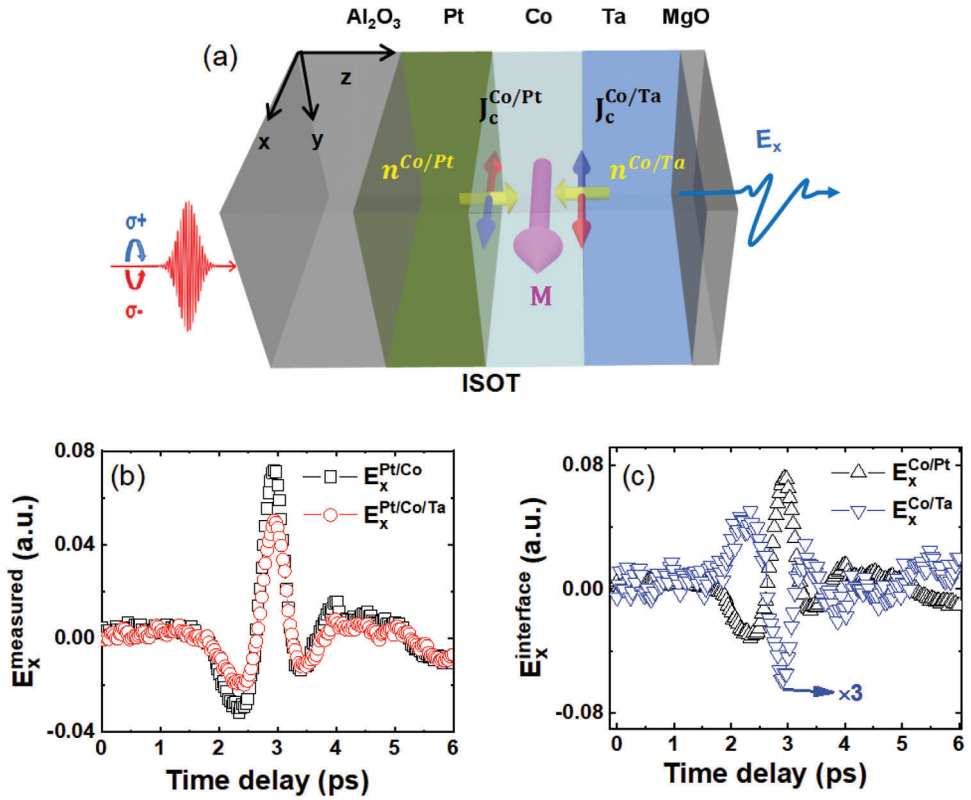

Figure 3. a) Schematic diagram of ISOT for trilayer case. b) E_x from Co/Pt bilayer and Pt/Co/Ta trilayer, measured at the THz detector. c) Estimated E_x at Co/Pt ($E_x^{Co/Pt}$, black) and Co/Ta interface ($E_x^{Co/Ta}$, blue). $E_x^{Co/Ta}$ is multiplied by three.

intensity also changes by flipping the sample. When the pump hits the substrate side (+**n**), it should pass through the Pt layer, losing 61% pump fluence by the reflection and absorption, resulting in the decrease of the pump-induced signal. The absorption coefficient of the Pt layer for the pump with 800-nm wavelength is estimated to be 0.505. Detailed intensity estimation is found in Section S1 (Supporting Information).

The effect of magnetization switching between positively (+M) and negatively (−M) saturated states in THz emission is shown in Figure 2c. As expected from the ISOT formula, switching of magnetization should lead to the opposite J_c, which is clearly observed in the figure shown in the case of the LCP pump (σ^-). The same trend, but with the opposite sign, is observed for the RCP (σ^+) pump. It has been known that the interface quality plays an important role in THz generation by ISOT. In the present study, pump-polarization-dependent THz emission by ISOT was observed for the films prepared in 7-mTorr Ar sputtering pressure, while no helicity-dependent THz emission was observed for the films prepared in 1-mTorr Ar sputtering pressure, as in Ref. [21].

ISOT contribution is also investigated for the trilayer (Pt/Co/Ta) film. The ISOT mechanism is schematically illustrated for the Pt/Co/Ta trilayer film in **Figure** 3a. Measured E_x profile ($E_x^{measured}$) for the bilayer and trilayer films are compared in Figure 3b for the case of $\sigma^+/+M/+n$. Overall E_x profile from the trilayer film is almost the same as the case of the bilayer except the intensity, where the intensity is smaller than the case of the bilayer. With the addition of the Ta layer, attenuation by the metallic Ta layer exists. Moreover, an extra interface effect should exist as well for the Co/Ta interface in addition to the Co/Pt interface. Considering the opposite n vector for Co/Ta and Co/Pt interfaces with the ferromagnetic Co layer in the middle, it is expected to see the reduced total ISOT effect in case of the trilayer film, as illustrated in the figure. It should be also mentioned that Ta has an opposite spin Hall angle compared to the Pt and thus, if the ISHE is involved in the THz emission, the intensity should be enhanced, rather than reduced for the trilayer as observed in the present case, indicating that the ISHE is irrelevant in this case. Moreover, ISHE as well as IREE should be detected for the THz emission polarization along the y-axis, not the x-axis, in the present geometry.

We would like to stress that the original THz emission from each interface can be quantified by consideration of attenuation factor of the multilayer structure for the pump laser so that the original THz wave emission along the x-axis ($E_x^{interface}$), when initially generated at the interface, is determined, as in Figure 3c. It is possible to compare the THz emissions from the bilayer and the trilayer films, where the larger $E_x^{measured}$ is observed for the bilayer case, as easily expected from the opposite sign of the normal vector (n) for the Co/Pt and Co/Ta interface. It is interesting to note that, however, the reduction of the $E_x^{measured}$ for the trilayer film is not significant, implying that ISOT contribution from the Co/Ta interface is fractional compared to the case of the Co/Pt interface. To separately quantify the ISOT contribution from Co/Ta and Co/Pt in the trilayer, it is assumed that the Co/Pt interface in the bilayer has the same amount

of contribution for THz emission in the trilayer. Then, by subtracting the Co/Pt interface contribution ($E_x^{Co/Pt}$) from the trilayer signal, the Co/Ta interface contribution ($E_x^{Co/Ta}$) is determined, as depicted in Figure 3c, where $E_x^{Co/Ta}$ is multiplied by three for comparison. The ISOT contribution ratio of the Co/Pt and the Co/Ta is found to be ≈3.5:1, similar to reported values based on the magnetoresistance method. For instance, the SOT strength ratio between Co/Pt and Co/Ta is estimated to be 3:1 for the Pt(6 nm)/Co(2.5 nm) and Ta(6 nm)/Co(2.5 nm) with in-plane magnetic anisotropy based on the ratio of field-like torques with the same component as ISOT in the present study.[28] On the other hand, for Co/Ta/Pt with perpendicular magnetic anisotropy, the field-like SOT efficiency is reported to be larger by 1.5 times than that of the Co/ Pt case.[29] In the case of CoFeB-based multilayers with perpendicular magnetic anisotropy, the transverse SOT effective field ratio between CoFeB/Pt and CoFeB/Ta is reported to be ≈1:2.[30] In addition to the above experimentally reported values based on the transport measurements at the Hall bar geometry, there has been a result reported for Co/Pt and Co/Ta films based on THz emission,[19] where the electric field profile of THz emission by ISOT is directly compared, as in the present work, and the ratio was ≈3:1. The samples in Ref. [19] has in-plane magnetic anisotropy, as in the present case, but has a thicker Co layer (10 nm) and a thinner heavy metal layer (2 nm), compared to the present samples Co(3 nm) and Pt, Ta(5 nm). Estimation of the ISOT strength from different interfaces is an important task, sensitively depending on the interface quality. We would like to state that the measurement by means of THz emission provides noncontacting optical way, not requiring making electrodes by patterning nor applying current.

Now, THz emission along the *y*-axis (E_y) is analyzed, where ISHE (**Figure** 4a) and IREE (Figure 4b) are supposed to play a key role in THz generation. First, for the bilayer film, it is observed that E_y is independent of pump polarization, as demonstrated in Figure 4c. E_y profile is found to be irrespective of the pump polarization, where the pump with LCP, RCP, and linear polarization (LP) exhibits almost the same profile, as shown in the figure for the case of **+M/+n**. The THz emission mechanism for E_y is considered to be ISHE and/or IREE, both of which are not pump-polarization dependent. On the other hand, IREE as well as ISHE sensitively depends on the multilayer interface quality. As observed by high-resolution cross-sectional transmission electron microscopy (Section S3, Supporting Information), while the interface quality of multilayers in the present study is not perfect, the multilayer heterostructure is still clearly sustained. We consider that ISOT and IREE might coexist in multilayer films.

Ultrafast demagnetization generates spin current into neighboring layers, then, the charge current (J_c) is induced by the ISHE, described as $J_c = \theta_{SH} \times J_s \times M/|M|$, where θ_{SH} is spin Hall angle, J_s is spin current originated from ultrafast demagnetization, and M is magnetization.[13–16] The detailed geometry of the sample and relevant quantities is illustrated in Figure 4a, where the spin current is denoted as $J_s^{Co/Pt}$. In the case of ISHE, the same amount of induced J_c regardless of the pump polarization is expected. Instead, it should be dependent on the direction of J_s and M. In the present sample, induced J_c in the Pt layer is only observable due to the high resistivity of MgO compared to the Pt. Therefore, by flipping the sample, the direction of J_s can be switched and thus, the induced J_c should be switched as well, as demonstrated by the opposite sign of E_y in Figure 4d. The relatively different phase by flipping is due to the different optical path, as in the case of 2(b). If M is reversed, E_y is accordingly reversed, as seen in Figure 4e. As in Figure 4f, the FFT of E_y profile shows the pump polarization-independent behavior.

IREE (Figure 4b) could also contribute to the THz emission along the *y*-axis.[17,18] According to the formula: $J_c = \lambda_{IREE}\, n \times S$[31], where λ_{IREE} is IREE coefficient, S is the nonequilibrium spin density due to the spin injection, parallel to M. n is the polar unit vector normal to the interface reflecting the inversion symmetry breaking, which is denoted as $n^{Co/Pt}$ in the figure. When J_s is injected into the neighboring Pt layer along the *z*-axis, an electric field along the *y*-axis is generated by the IREE, proportional to $J_s \times M$. Spins along +x direction (−x direction) with + M ($-M$) are accumulated along +y direction (−y direction), resulting in spin current $J_s^{Co/Pt}$ and charge current $J_c^{Co/Pt}$ along the y-axis, as illustrated in the figure.[31,32] As in the case of the ISHE, IREE does not have the pump-polarization dependence. By flipping the sample, only n is changed, while S is invariant by the external magnetic field, resulting in the THz emission profile with an opposite phase, as observed in the case of Figure 4d. The larger amplitude of E_y when excited by the pump on the film side (**−n**), is explainable by the higher pump intensity, as in the case of Figure 2b. Also, the pump-induced THz emission signal is reduced for the (**+n**) case when the THz wave passes through the Co/MgO layers, as in the case of 2(b). Detailed intensity estimation for E_y is found in Sections S1 and S2 (Supporting Information). In the case of IREE, E_y is also symmetrically switched by reversing M, as seen in Figure 4e. In Figure 4f, the FFT of THz emission profiles in the case of RCP, LCP, and LP pump, are plotted, where the almost same FFT spectra are observed. It is considered that the spin-charge conversion mechanisms might be sensitively dependent on the film interface quality. Recently, the Rashba-type spin splitting and spin-charge conversion phenomenon has been investigated in Pt/Co/W films.[33]

To distinguish ISHE and IREE mechanisms, THz emission along the y-axis (E_y) is analyzed for the trilayer film. Both ISHE and IREE are expected to coexist as in the case of bilayer film, where the additional contribution from the Co/Ta interface is investigated. Schematic diagrams of ISHE and IREE mechanisms in trilayer are illustrated in **Figure** 5a,b, respectively. In the case of ISHE, since Ta has an opposite spin Hall angle (θ_{SH}) compared to Pt,[13,15,16] it is expected to have THz emission amplitude by ISHE is stronger than the case of bilayer due to the same direction of J_c from Co/Pt and Co/Ta interfaces. On the other hand, J_c generated by IREE from Co/Pt and Co/Ta interfaces are opposite in direction to each other due to the mutually opposite normal vector toward Co layer from Pt and Ta heavy metal layers.[19] The measured E_y with combined contributions from ISHE and IREE for the bilayer and the trilayer is plotted in Figure 5c. Since E_y does not have pump-polarization dependency, average of E_y pumped by LCP and RCP is considered. The $E_y^{measured}$, measured amplitude for the trilayer at the THz detector is larger than the case of the bilayer, clearly indicating that the contribution from ISHE is larger than that of IREE in the Pt/Co/Ta trilayer.

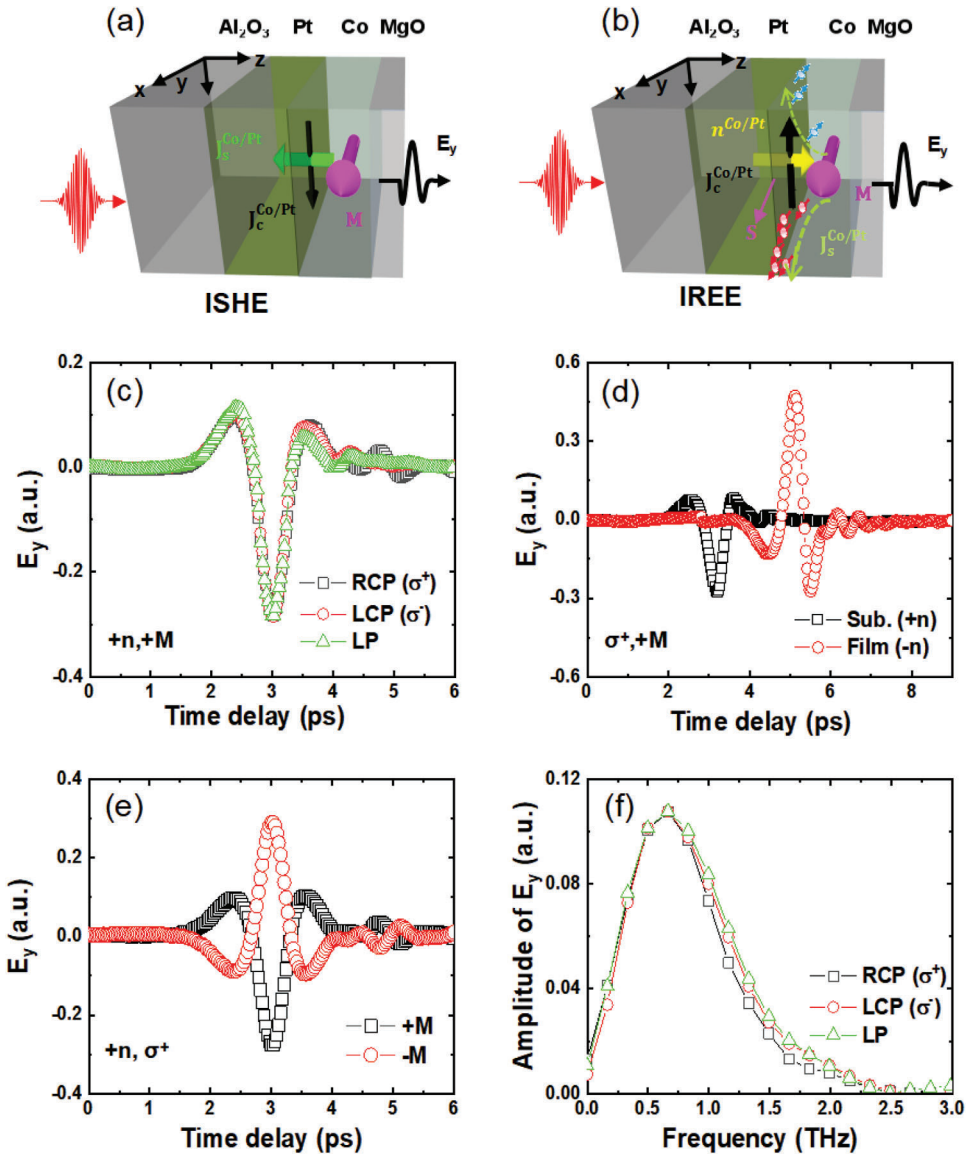

Figure 4. Schematic diagram of (a) ISHE and (b) IREE mechanism for Co/Pt sample. c) E_y generated by LCP, RCP, and LP for the case of +**M** and +**n**. d) E_y with pump incident from the substrate (+**n**) and the film side (−***n***) for the case of σ^+ and +***M***. e) E_y for +***M*** and −*M* for the case of +***n*** and σ^+. f) FFT of E_y for LCP, RCP, and LP pump.

To quantitatively separate the ISHE and IREE THz emission generated at each interface along the *y*-axis, $E_y^{interface}$ is estimated in analogous to the case of $E_x^{interface}$ in Figure 3. Note that the difference between the bilayer and the trilayer cases is still sustained. In analogous to the case of Figure 3c, $E_y^{Co/Pt}$ and $E_y^{Co/Ta}$ are also estimated as in Figure 5d. It is interesting to note that the $E_y^{Co/Pt}$ is much larger than $E_y^{Co/Ta}$, roughly by 6.5 times. It should be mentioned that $E_y^{interface}$ originated from ISHE and IREE has the opposite sign at the Co/Pt interface, whereas $E_y^{interface}$ from ISHE and IREE has the same sign at the Co/Ta interface. Due to the larger θ_{SH} for Pt (≈0.1) compared to Ta (0.12–0.0037),[25,34,35] $E_y^{Co/Pt}$ is expected to be larger than $E_y^{Co/Ta}$. Moreover, the same sign of IREE contribution at the Co/Ta interface increases $E_y^{Co/Ta}$ further, while ISHE is stronger overall than IREE in the present sample, as observed by the same phase of the total E_y in Figure 5d. All our observations imply that the $E_y^{Co/Ta}$(ISHE) is substantially less than $E_y^{Co/Pt}$(ISHE), as discussed in Section S2 (Supporting Information).

The ratio between $E_y^{Co/Pt}$(ISHE) and $E_y^{Co/Ta}$(ISHE) should be proportional to the ratio between θ_{SH} of Pt and Ta, assuming that the J_s by the ultrafast demagnetization to the Pt layer and the Ta layer are almost the same. On the other hand, it has been known that the field-like ISOT originated from the Rashba effect[36,37] so the ratio of E_y originating from the IREE between the Co/Pt and Co/Ta interfaces is assumed to be proportional to the ratio of E_x originated from the ISOT at the two interfaces, which was measured as in Figure 3c. A 3.5:1 ratio is taken for the values

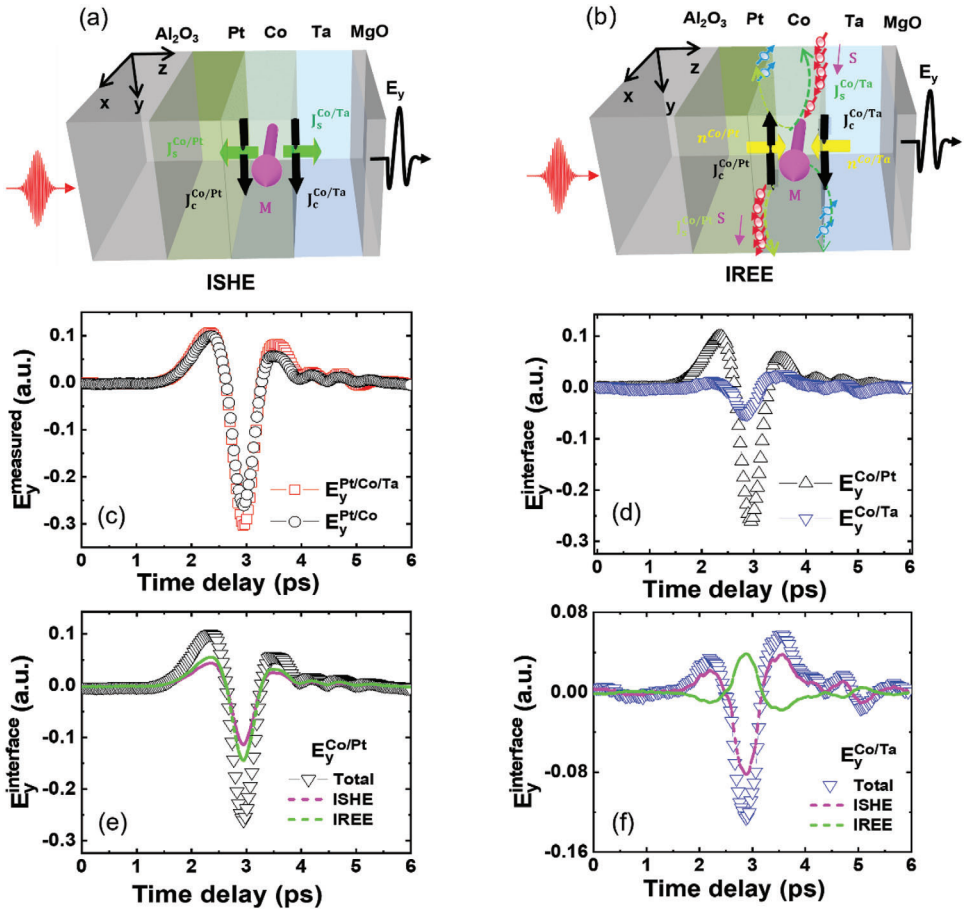

Figure 5. Schematic diagram of (a) ISHE and (b) IREE for Pt/Co/Ta multilayer. c) E_y from Pt/Co bilayer and Pt/Co/Ta trilayer, measured at the THz detector. d) Estimated E_y at Co/Pt ($E_y^{Co/Pt}$, black) and Co/Ta interface ($E_y^{Co/Ta}$, blue). Total E_y originally generated at (e) Co/Pt and (f) Co/Ta interface with separated contribution from ISHE and IREE.

estimated at the original THz source position at the interface. Combining all the information, ISHE and IREE contribution ratio of Co/Pt and Co/Ta interfaces, $E_y^{Co/Pt}$(ISHE), $E_y^{Co/Ta}$(ISHE), $E_y^{Co/Pt}$(IREE), and $E_y^{Co/Ta}$(IREE) are all separately estimated. In Figure 5e, $E_y^{Co/Pt}$(ISHE) and $E_y^{Co/Pt}$(IREE) are plotted together, where it is observed IREE contribution is larger than ISHE contribution for Co/Pt interface. Similarly, in Figure 5f, $E_y^{Co/Ta}$(ISHE) and $E_y^{Co/Ta}$(IREE) are plotted, where ISHE contribution is larger than IREE contribution. Note that the IREE signal has the same phase as the ISHE signal. Detailed calculation for Figure 5e,f is found in Section S2 (Supporting Information).

Finally, we summarize the quantified contribution from the three main spin-charge conversion mechanisms for THz emission at the embedded Co/Pt and Co/Ta interface in Pt/Co/Ta trilayer film. The strength ratio among ISHE, IREE, and ISOT at the Co/Pt interface is found to be ≈1.6:2:1, respectively. The ratio at the Co/Ta interface is ≈3.9:2:1. IREE contribution is most significant at the Co/Pt interface, followed by ISHE and ISOT, while ISHE contribution is the largest and the ISOT becomes relatively fractional at the Co/Ta. Considering that the ISHE is mainly initiated by the spin current from the Co layer to the Pt and Ta layers by ultrafast demagnetization, the substantial amount of ISHE contribution both for Co/Pt and Co/Ta interface cases is understandable. It is interesting to see the contrasting difference in IREE contribution, which is even larger than the ISHE at the Co/Pt interface but much smaller than the ISHE at the Co/Ta interface. The spin-charge conversion efficiency can be roughly approximated to be proportional to a spin diffusion length l_{sd} as well as θ_{SH}.[38] l_{sd} of Pt and Ta have been reported to be ≈11 and 2.7 nm, respectively.[35] Then, the ratio of $\theta_{SH} \times l_{sd}$ between Pt (0.1 × 11 nm) and Ta (0.07 × 2.7 nm) from scattered reported values[25,35,36] is ≈6:1, which is consistent with 3.5:1 ratio in IREE and ISOT ratio measured in the present study.

3. Conclusion

In summary, we have systematically investigated THz emission in Co/Pt and Pt/Co/Ta magnetic multilayers triggered by ultrafast pump pulse with polarization control. By compensating the absorption for the pump laser and subtracting the THz emission signal of the bilayer from the signal of the trilayer, the THz emission generated from each interface is quantitatively identified. Furthermore, spin-charge conversion by ISOT, ISHE, and IREE is distinguishably estimated at the embedded Co/Pt and Co/Ta interfaces. Our approach sheds light on the realization of

the broadband spintronic emitter, providing quantitative analysis to separately understand different THz generation mechanisms coexisting in various magnetic multilayers.

Supporting Information

Supporting Information is available from the Wiley Online Library or from the author.

Acknowledgements

This research was supported by the Commercialization Promotion Agency for R&D Outcomes(COMPA) funded by the Ministry of Science and ICT(MSIT). (1711198544, Development of analytical instrumentation for electromagnetics/optics/thermal characteristics under extreme environment). This research was also supported by the National Research Foundation of Korea (RS-2023-00250178). KWK acknowledges the Basic Science Research Program through the National Research Foundation of Korea (NRF) (NRF-2020R1A2C3013454). Structural analysis of samples was conducted at the Instrumentation and Service Center for Physical Sciences in Westlake University. The authors also thank Dr. Yangjian Lin at Westlake University for his assistance in the structural analysis based on electron microscopy.

Conflict of Interest

The authors declare no conflict of interest.

Data Availability Statement

The data that support the findings of this study are available from the corresponding author upon reasonable request.

Keywords

inverse Rashba–Edelstein effect, inverse spin Hall effect, inverse spin-orbit torque, spin-charge conversion, THz spintronics

Received: October 10, 2023
Revised: March 27, 2024
Published online: April 9, 2024

[1] J. Walowski, M. Münzenberg, *J. Appl. Phys.* **2016**, *120*, 140901.
[2] T. Kampfrath, A. Sell, G. Klatt, A. Pashkin, S. Mährlein1, T. Dekorsy, M. WolF, M. Fiebig, A. Leitenstorfer, R. Huber1, *Nat. Photonics* **2011**, *5*, 31.
[3] T. Seifert, S. Jaiswal, U. Martens, J. Hannegan, L. Braun, P. Maldonado, F. Freimuth, A. Kronenberg, J. Henrizi, I. Radu, E. Beaurepaire, Y. Mokrousov, P. M. Oppeneer, M. Jourdan, G. Jakob, D. Turchinovich, L. M. Hayden, M. Wolf, M. Münzenberg, M. Kläui, T. Kampfrath, *Nat. Photonics* **2016**,*10*, 483.
[4] T. Kampfrath1, M. Battiato, P. Maldonado, G. Eilers, J. Nötzold, I. Radu, F. Freimuth, Y. Mokrousov, S. Blügel, M. Wolf, P. M. Oppeneer, M. Münzenberg, *Nat. Nanotechnol.* **2013**, *8*, 256.
[5] E. T. Papaioannou, R. Beigang, *Nat. Photonics* **2020**, *10*, 1243.
[6] E. Beaurepaire, G. M. Turner, S. M. Harrel, M. C. Beard, J.-Y. Bigot, C. A. Schmuttenmaer, *Appl. Phys. Lett.* **2024**, *84*, 3465.
[7] N. Kumar, R W. A. Hendrikx, A J. L. Adam, P C. M. Planken, *Opt. Express.* **2015**, *23*, 14252.
[8] R. Rouzegar, L. Brandt, L. Nádvorník, D A. Reiss, A L. Chekhov, O. Gueckstock, C. In, M. Wolf, T S. Seifert, P W. Brouwer, G. Woltersdorf, T. Kampfrath, *Phys. Rev. B* **2022**, *106*, 144427.
[9] L. Huang, S.-H. Lee, S. D. Kim, Je-Ho Shim, H. J. Shin, S. Kim, J. Park, S. Y. Park, Y. S. Choi, H.-J. Kim, J-Il. Hong, D. E. Kim, D.-H. Kim, *Sci. Rep.* **2020**, *10*, 15843.
[10] L. Huang, J.-W. Kim, S-H. Lee, S-D. Kim, V. M. Tien, K. P. Shinde, Je-Ho S Y. Shin, H. J. Shin, S. Kim, J. Park, S.-Y. Park, Y. S. Choi, H.-J. Kim, J-Il Hong, D. E. Kim, D.-H. Kim, *Appl. Phys. Lett.* **2019**, *115*, 142404.
[11] L. Cheng, Z. Q. Li, D. M. Zhao, E E. M. Chia, *APL Mater.* **2021**, *9*, 070902.
[12] T. H. Dang, J. Hawecker, E. Rongione, G. Baez Flores, D. Q. To, J. C. Rojas-Sanchez, H. Nong, J. Mangeney, J. Tignon, F. Godel, S. Collin, P. Seneor, M. Bibes, A. Fert, M. Anane, J.-M. George, L. Vila, M. Cosset-Cheneau, D. Dolfi, R. Lebrun, P. Bortolotti, K. Belashchenko, S. Dhillon, H. Jaffrès, *Appl. Phys. Rev.* **2020**, *7*, 041409.
[13] Y. Wu, M. Elyasi, X. Qiu, M. Chen, Y. Liu, L. Ke, H. Yang, *Adv. Mater.* **2017**, *29*, 1603031.
[14] D. Yang, J. Liang, C. Zhou, L. Sun, R. Zheng, S. Luo, Y. Wu, J. Qi, *Adv. Optical Mater.* **2016**, *4*, 1944.
[15] T. Seifert, S. Jaiswal, M. Sajadi, G. Jakob, S. Winnerl, M. Wolf, M. Klaui, T. Kampfrath, *Appl. Phys. Lett.* **2017**, *110*, 252402.
[16] S. Kumar, A. Nivedan, A. Singh, S. Kumar, *Pramana – J. Phys.* **2021**, *95*, 75.
[17] C. Zhou, Y. P. Liu, Z. Wang, S. J. Ma, M. W. Jia, R. Q. Wu, L. Zhou, W. Zhang, M. K. Liu, Y. Z. Wu, J. Qi, *Phys. Rev. Lett.* **2018**, *121*, 086801.
[18] M B. Jungfleisch, Q. Zhang, W. Zhang, J E. Pearson, R D. Schaller, H. D. Wen, A. Hoffmann, *Phys. Rev. Lett.* **2018**, *120*, 207207.
[19] T. J. Huisman, R. V. Mikhaylovskiy, J. D. Costa, F. Freimuth, E. Paz, J. Ventura, P. P. Freitas, S. Blügel, Y. Mokrousov, Th. Rasing, A. V. Kimel, *Nat. Nanotechnol.* **2016**, *11*, 455.
[20] G. Li, R. V. Mikhaylovskiy, K. A. Grishunin, J. D. Costa, T. Rasing, A. V. Kimel, *J. Phys. D: Appl. Phys.* **2018**, *51*, 134001.
[21] G. Li, R. Medapalli, R. V. Mikhaylovskiy, F. E. Spada, T. Rasing, E. E. Fullerton, A. V. Kimel, *Phys. Rev. Mater.* **2019**, *3*, 084415.
[22] G. Torosyan, S. Keller, L. Scheuer, R. Beigang, E. T. Papaioannou, *Sci. Rep.* **2018**, *8*, 1311.
[23] A. Comstock, M. Biliroglu, D. Seyitliyev, A. McConnell, E. Vetter, P. Reddy, R. Kirste, D. Szymanski, Z. Sitar, R. Collazo, K. Gundogdu, D. Sun, *Adv. Optical Mater.* **2023**, *11*, 2201535.
[24] J. Hawecker, E. Rongione, A. Markou, S. Krishnia, F. Godel, S. Collin, R. Lebrun, J. Tignon, J. Mangeney, T. Boulier, J.-M. George, C. Felser, H. Jaffrès, S. Dhillon, *Appl. Phys. Lett.* **2022**, *120*, 122406.
[25] A. Hoffmann, *IEEE Trans. Magn.* **2013**, *49*, 5172;
[26] J. Park, C. Kim, J. Lee, C. Yim, C. H. Kim, J. Lee, S. Jung, J. Ryu, H.-S. Kang, T. Joo, *Rev. Sci. Instrum.* **2011**, *82*, 013305.
[27] P. Koleják, G. Lezier, K. Postava, J.-F. Lampin, N. Tiercelin, M. Vanwolleghem, *ACS Photonics* **2022**, *9*, 1274.
[28] Y. Du, H. Gamou, S. Takahashi, S. Karube, M. Kohda, J. Nitta, *Phys. Rev. Applied* **2020**, *13*, 054014.
[29] K.-F. Huang, D.-S. Wang, H.-H. Lin, C.-H. Lai, *Appl. Phys. Lett.* **2015**, *107*, 232407.
[30] W. Fan, J. Zhao, M. Tang, H. Chen, H. Yang, W. Lü, Z. Shi, X. Qiu, *Phys. Rev. Appl.* **2019**, *11*, 034018.
[31] J. Shen, Z. Feng, P. Xu, D. Hou, Y. Gao, X. Jin, *Phys. Rev. Lett.* **2021**, *126*, 197201.
[32] A. Manchon, H. C. Koo, J. Nitta, S. M. Frolov, R. A. Duine, *Nat. Mater.* **2015**, *14*, 871.
[33] W. S. Ham, T. H. Ho, Y. Shiota, T. Iino, F. Ando, T. Ikebuchi, Y. Kotani, T. Nakamura, D. Kan, Y. Shimakawa, T. Moriyma, E. Im, N.-J. Lee, K.-W. Kim, S. C. Hong, S. H. Rhim, T. Ono, S. Kim, *Adv. Sci.* **2023**, *10*, 2206800.

[34] H. L. Wang, C. H. Du, Y. Pu, R. Adur, P. C. Hammel, F. Y. Yang, *Phys. Rev. Lett.* **2014**, *112*, 197201.
[35] M. Morota, Y. Niimi, K. Ohnishi, D. H. Wei, T. Tanaka, H. Kontani, T. Kimura, Y. Otani, *Phys. Rev. B* **2011**, *83*, 174405.
[36] A. V. Khvalkovskiy, V. Cros, D. Apalkov, V. Nikitin, M. Krounbi, K. A. Zvezdin, A. Anane, J. Grollier, A. Fert, *Phys. Rev. B* **2013**, *87*, 020402.
[37] A. Kalitsov, S. A. Nikolaev, J. Velev, M. Chshiev, O. Mryasov, *Phys. Rev. B* **2017**, *96*, 214430.
[38] Y. Li, S. Yang, D. Sun, Y. Sun, Y. Li, E. Vetter, R. Sun, N. Li, X. Yang, L. Su, Z. Gong, Z. Xie, J. Zhao, W. He, X. Zhang, Z. Cheng, *Phys. Rev. B* **2020**, *102*, 014420.